Reply to Referee # 1

The authors thank the reviewer for his pertinent and helpful comments on the paper and they are grateful for his review which is always rather time-consuming and cumbersome. The manuscript has been modified according to the suggestions proposed by the reviewer. The remainder is devoted to the specific response item-by-item of the reviewer's comments :

Major Comments :

1. The main results obtained during previous observations in mixed-phase Arctic clouds are now referenced in the introduction with a discussion about the modeling studies on ice formation mechanisms published in the last years. Therefore, the observations acquired during the ASTAR 9 April case study are placed in the context of the existing body of literature on the characterization of Arctic mixed-phase clouds.

2. In this paper the cloud microphysical measurements are reported from a PMS FSSP, a Polar Nephelometer and a Cloud Particle Imager. Without available PMS 2D-C measurements the CPI data were used in order to derive the particle size distributions and the microphysical parameters as Gallagher et al. (2005) in cirrus clouds. Cloud particle sizes, when inferred from images taken with this instrument, are oversized with regards to the true dimension. Furthermore, the subsequent distances on which the particles are accepted in the image frame are greater than the depth of field from the object plane. Therefore, large uncertainties occur on derived size distributions particularly for particles smaller than about 100 μm. In order to reduce these errors, a calibration method was devised (Connolly et al., 2007) from optical bench measurements which use calibrated glass beads and ice analogs. The CPI operated during ASTAR 2004 and ASTAR 2007 campaigns (see Engvall et al., 2008) was calibrated by applying this method at the University of Manchester (Lefèvre, 2007). As reported in a previous paper (Gayet et al., 2009), the calibration results were conclusively validated by comparing the CPI size distributions to the 2D-C data during the ASTAR 2004 campaign. Following a similar way the CPI measurements were also compared to PMS 2D-C and 2D-P data during the POLARCAT 2008 experiment (Law et al., 2008) still in Arctic layer clouds. We note in passing the ATR42 aircraft used during POLARCAT has very similar performances (in terms of airspeed) of the Polar2 aircraft operated during ASTAR. Therefore we may reasonably assume that the CPI validations performed from the POLARCAT data are relevant for the results presented in this study. Figs. A1.a and A1.b displays the results obtained during POLARCAT in a Nimbostratus cloud near -25°C and in a boundary layer mixed-phase cloud near -15°C, respectively. A very good agreement is found between the size distributions for both examples with mostly bullet-Rosette ice crystal shape (Fig. A1.a) and rimed particles (Fig. A1.b). Mean values of the concentration of particles with D> 100 μm, extinction coefficient and ice water content are also reported on Fig. A1 for CPI probe and both PMS 2D-C & 2D-P instruments. The discrepancies between the two probes are undoubtedly within the large uncertainties expected for the PMS instruments (up to 75% and 100% on particle concentration and ice water content respectively, see Gayet et al., 2002) and confirm the previous comparisons results (Gayet et al., 2009). Therefore, we consider the errors on the size distributions and derived microphysical parameters calculated from the (calibrated) CPI are of the same order of those from the PMS instruments. Annex A was added in the revised manuscript in order to explain the above statements.

Minor comments :

1. See revised version.

2. Id°

3. Id°

4. During ASTAR 2007 no direct LWC measurements (King Probe, …) were available. Hovewer, in order to check the consistency of liquid water droplet measurements we systematically compared the FSSP and Polar Nephelometer information. Figure A2 displays the comparison between the extinction coefficient derived from the Polar Nephelometer (see Gayet et al., 2002) and the FSSP. These results concern in-cloud sequences where only (supercooled) water droplets were present (i.e. no ice particles were detected by the CPI) and assuming non-absorbing droplets. A very good agreement is observed between the two independent measurements which indicates the consistency of the results. This consistency is nicely confirmed in comparing the measured scattering phase function (Polar Nephelometer) and the one obtained by Mie theory calculated with the averaged droplet size distribution measured by the FSSP with data reported on Fig. A2 (see Fig. A3, right panel; see also Fig. 3.b in the manuscript). Direct FSSP size distribution and retrieved droplet size spectrum obtained by using the inverse-method of Oshchepkov et al. (1993) from the measured scattering phase function also fit very well. Direct and inverse microphysical parameters are also indicated on Fig. A3.

5. The use of normalized altitude is a good representation when comparing vertical profiles with different clouds (McFarquhar et al., 2007). Nevertheless, the aim of the results on Figs. 3a and 4a is to perform qualitative comparisons with CALIPSO and CloudSat profiles.

6. As Fu (1996) and Francis et al. (1994) the effective diameter definition in this study is proportional to the volume/area ratio of ice crystals. According to McFarquhar and Heymsfield (1998) large effective diameter (as defined above) does not necessarily reveal the existence of large ice crystals. Figure A4 represents the mean volume diameter [i.e. Σ iwc(i)*d(i) / Σ iwc(i)] versus the effective diameter, both parameters being calculated from the CPI data. The relationship between the two diameters observed on Fig. 4 indicates that in our case study large ice crystals are described by large values of the effective diameter.

7. The paper describes the results obtained during a case study and do not represent a large data set as those described by Korolev et al. (1999) and by McFarquhar et al. (2007). Furthermore the results of the shape particle classification (from CPI images) are strongly dependent on the algorithms used in the recognition methods via different. For instance Korolev et al. considered only two main particles shapes: pristine (faceted single crystals) and found that 98% of ice crystal observed in the Arctic were irregular. Our results on Fig. 5 illustrate that a more detailed classification can be made and show that ‘pristine’ ice crystals (single columns and plates) dominate (~ 50%) the particle shape near -20°C. Differences in ice particle shapes are found with regards to the results by MacFarquhar et al. (2007) in a

similar temperature range from -12°C to -15°C. They mostly observed rosette shapes whereas prevalent dendrites (~ 40%) with fewer rosette shape (10%) characterize our case study.

8. The FSSP droplet size distribution displayed on Figs. 3b (liquid water-phase) can be compared to the results of McFarquhar and Cober (2004) in water part of mixed-phase clouds (their Fig. 2). It is interesting to note that the two size distributions are similarly peaked, which would offer one more evidence that the FSSP is responding to water. The very good agreement between the scattering phase functions from FSSP + Mie theory and Polar Nephelometer (Fig. 3b, right panel) is a strong argument in this way. In section 3.3 (lines 12-15), we claim that broadband radiative effects are dominated by the water phase which is in agreement with the findings of MacFarquhar and Cober (2004).

9. See Appendix A about CPI / 2D-C comparisons.

10. In order to discuss about the liquid fraction (*fl*) we have reported on Fig. A5 the liquid fraction (fl = LWC / (LWC + IWC) as a function of the asymmetry parameter for the 9 April (this case study) and for the 7 April (left and right panels respectively). The right panel of Fig. A5 clearly shows that the cloud typically had *fl* <0.2 or *fl* > 0.8 with rather few values in between as already observed by Cober et al. (2001), Korolev et al. (2003) and MacFarquhar et al. (2007). This situation corresponds to an (Arctic) mixed-phase cloud layer with quasi constant top level near -20°C. Concerning the 9 April case the *fl* distribution is significantly different with fl ranging between 0.2 and 0.6 for asymmetry parameter values related to ice particles (<0.8). Most of the data point with 0.2 < *fl* < 0.8 correspond to the observations carried out through the high echo core (see Fig. 4a) with numerous large ice crystals (up to 800 l-1). Therefore the FSSP-100 measurements were likely contaminated by ice crystal shattering leading to overestimated *LWC* values and subsequent *fl* values.

11. The ice crystals were observed with sizes up to 2.1 mm in the high echo core region.

12. Annex B is added in the manuscript in order to present the Algorithm for Reflectivity factor derivation from CPI data.

The radar equivalent reflectivity factor is calculated by using the following relationship (Liu and Illingworth, 2000, Hogan et al., 2005, Protat et al., 2007):

$$Z(mm^6 m^{-3}) = 10^{15} \frac{|K_i|^2}{|K_w|^2} \sum_{j,D} \left(\frac{\rho_{eq(j,D)}}{\rho_g} \right)^2 N_{j,D}(D) D^{\ 6} f\ (D)$$

$$Z(dBZ) = 10\ \log Z(mm^6 m^{-3})$$

with:

- K_i and K_w the dielectric factors of ice at 94 GHz (0.177) and water (0.75) respectively;

● $\left(\frac{\rho_{eq(j,D)}}{\rho_g} \right)$ is the ratio of the equivalent density of ice crystal to the solid ice density in order to take into account the effects of shape and density of ice crystals (Oguchi, 1983). ρ_{eq} is determined according to the shape (j) of the particles recognized from the CPI images (Lefèvre, 2007) and to the corresponding mass-diameter relationships (Locatelli and Hobbs 1974, Mitchell, 1996). ρ_g = 0.9 g cm^{-3};

● $N_{j,D}$ *(D)* is the concentration of particles (l^{-1}) with the shape j and diameter *D (μm);*

● *f(D)* represents the ratio of the Mie scattering to the Rayleigh scattering at 94 GHz which depends the particle diameter in order to take into account the effects of Mie scattering when the particles are larger than 600 μm (see Boudala et al., 2006).

13. Regarding the comments about the spatial scale and the differences between ECMWF and observations there are two issues:

- Did ECMWF resolve the mesoscale structure of the observed clouds? ECMWF has a spatial horizontal resolution of about 20 km; the vertical resolution amounts to about 200 m in the boundary layer and the temporal resolution is 6 hours! This is certainly much coarser than the in-situ and remote-sensing observations. Nevertheless, the general transition from those clouds associated with the ceasing cold air outbreak to the deeper boundary layer clouds is represented very well as can be seen by the CWC field in Fig. 9. This implies that the weather situation didn't change much between the both analyses times 06 and 12 UTC. However, the smaller scale vertical updrafts along the flight path are not resolved and they cannot be resolved as the ECMWF doesn't simulate explicitly shallow convection (it is a hydrostatic model).

- Do the not-resolved vertical velocities influence the partitioning between cloud ice and cloud water? In principle, we would guess so. On the other hand, ECMWF is using a rather simple microphysical scheme for all clouds. Thus, a necessary next step to answer this question would be to apply more advanced microphysical schemes in cloud-resolving mesoscale models. In the context of the ECMWF it doesn't make sense! But, in principle, we think that the spatial scale plus the microphysical scheme influence the comparison of modelled and observed cloud properties!

The final question cannot be answered in our paper. This is certainly a relevant question but requires a thorough study of all possible impacts (SST, wind field, moisture, aerosols. ...). However, the main point is that the current microphysical scheme at ECMWF is not appropriate for Arctic mixed-phase clouds.

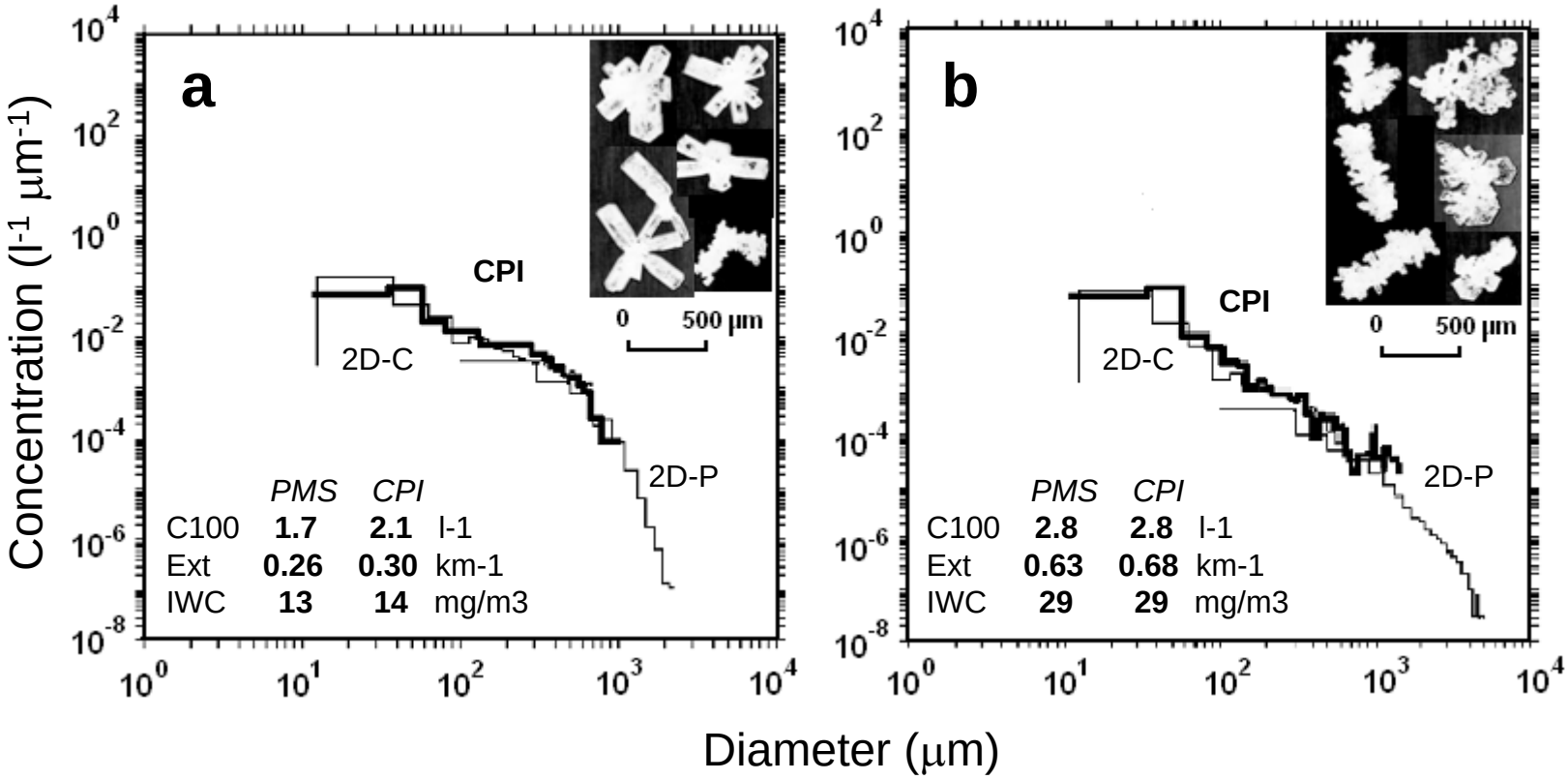
a
b
CPI
2D-C
2D-P
0 500 µm
PMS CPI
C100 1.7 2.1 l-1
Ext 0.26 0.30 km-1
IWC 13 14 mg/m3
C100 2.8 2.8 l-1
Ext 0.63 0.68 km-1
IWC 29 29 mg/m3
Concentration (l-1 µm-1)
Diameter (µm)

Figure A1

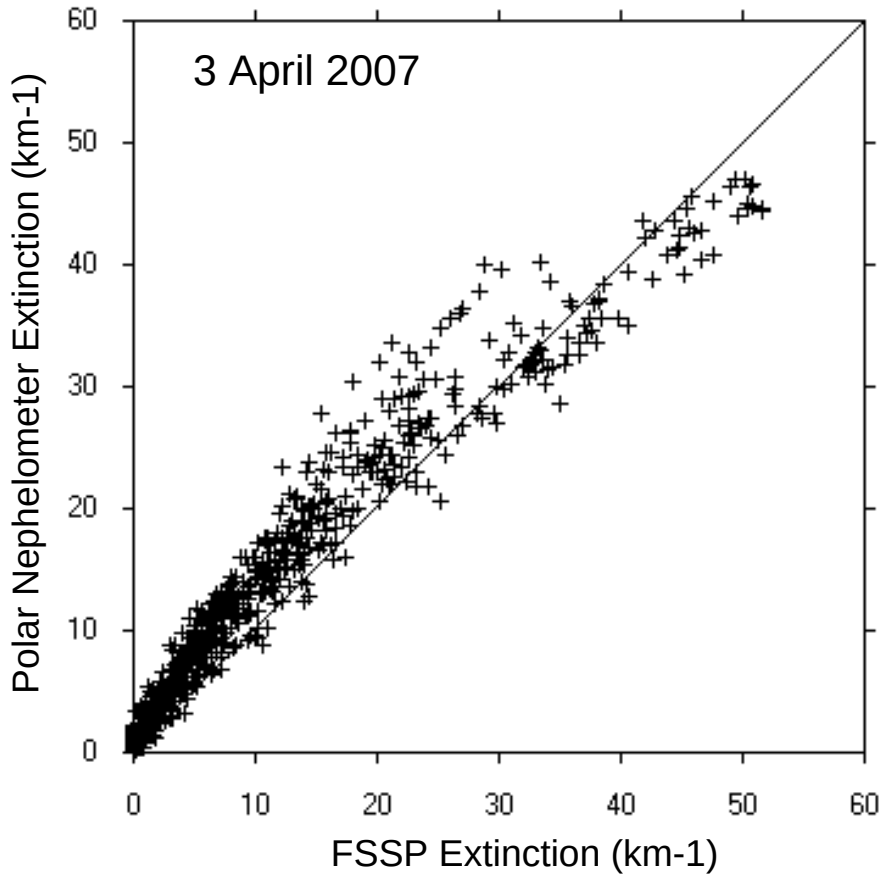
3 April 2007
Polar Nephelometer Extinction (km-1)
FSSP Extinction (km-1)
0
10
20
30
40
50
60

Figure A2

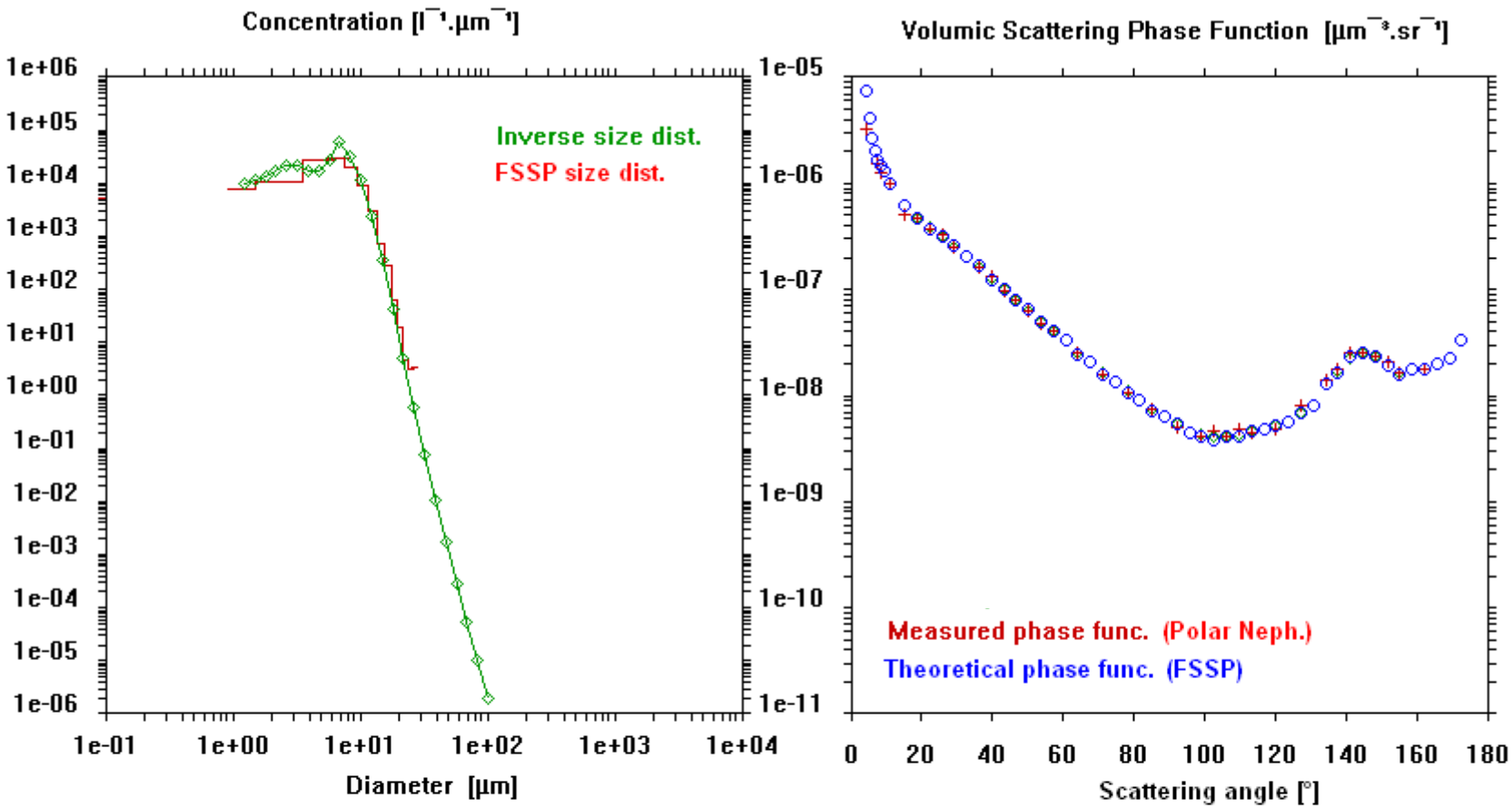

ConcFssp = 217.3 cm-3	ConcInv = 248.6 cm-3	err = 14.4 %
LWCFssp = 0.052 g/m3	LWCInv = 0.050 gm-3	err = -3.9 %
DmFssp = 9.8 µm	DmInv = 6.4 µm	err = -35.0 %
DeffFssp = 11.3 µm	DeffInv = 8.1 µm	err = -28.1 %
ExtFssp = 17.2 km-1	ExtInv = 18.3 km-1	err = 6.0 %

3 April 2007

Figure A3

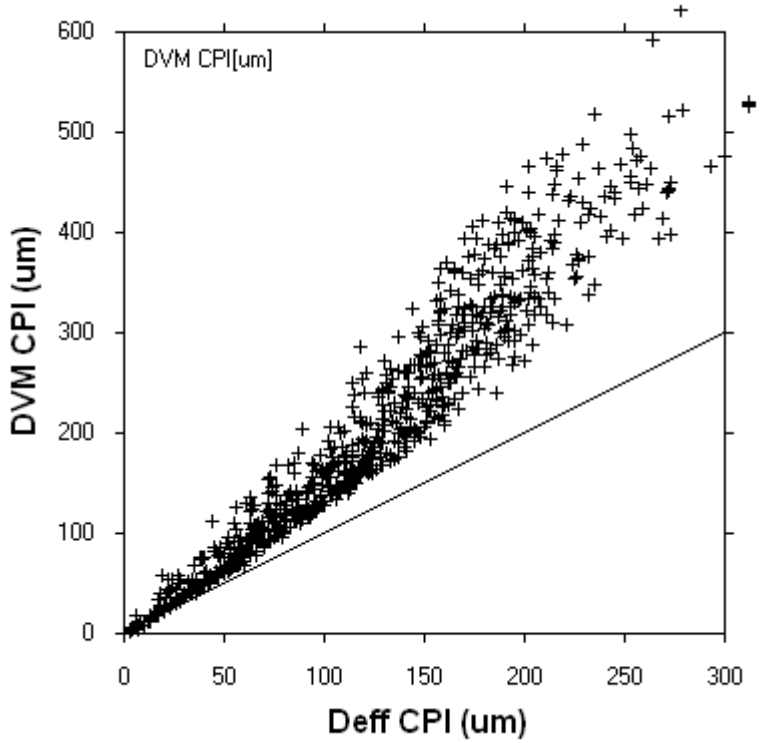
DVM CPI[um]
DVM CPI (um)
Deff CPI (um)
0
100
200
300
400
500
600
0
50
100
150
200
250
300

Figure A4

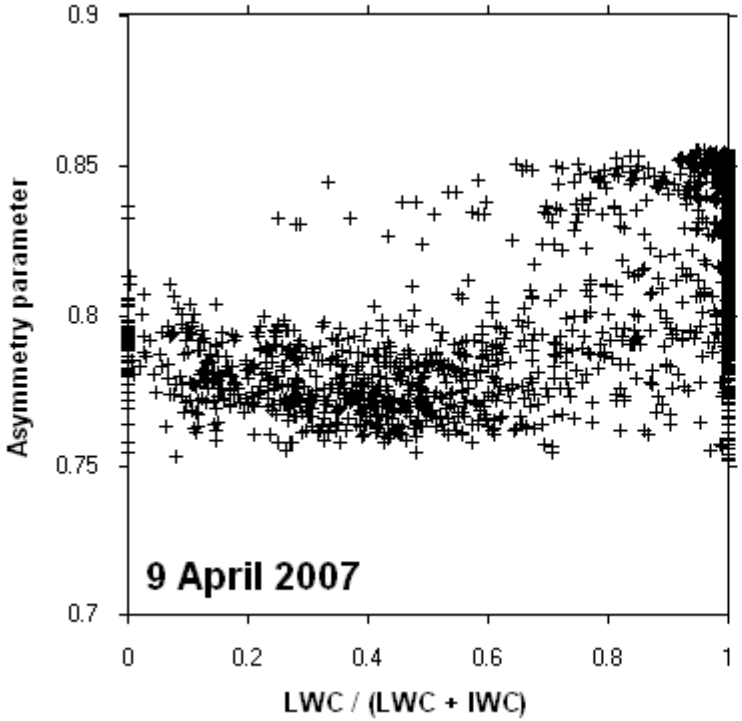
0.9
0.85
0.8
0.75
0.7
Asymmetry parameter
9 April 2007
0
0.2
0.4
0.6
0.8
1
LWC / (LWC + IWC)

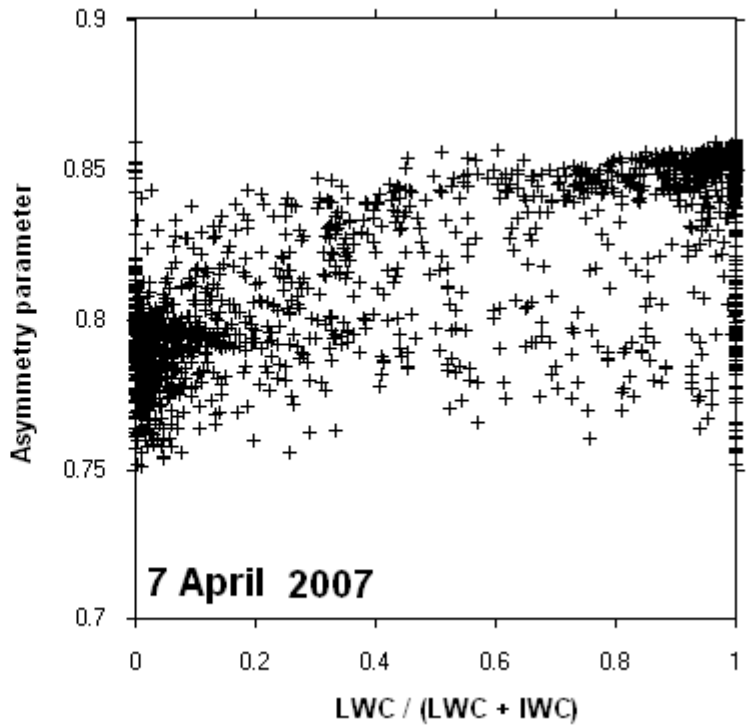
0.9
0.85
0.8
0.75
0.7
Asymmetry parameter
7 April 2007
0
0.2
0.4
0.6
0.8
1
LWC / (LWC + IWC)

Figure A5